Two-dimensional turbulence and dispersion in a freely decaying system

A. E. Hansen,* D. Marteau, and P. Tabeling
Laboratoire de Physique Statistique, École Normale Supérieure, 24 rue Lhomond, 75231 Paris, France
(Received 8 October 1997; revised manuscript received 12 March 1998)

We report experimental results obtained on freely decaying two-dimensional turbulence. The flow is produced in a thin stratified layer of electrolyte, using an electromagnetic forcing. The velocity and vorticity fields are measured using a particle image velocimetry technique. The study of the temporal evolution of the system confirms in detail the scaling theory of Carnevale *et al.* [Phys. Rev. Lett. **66**, 2735 (1991)]; the experimental value we find for the exponent characterizing the decay of the vortex density is $\xi = 0.7 \pm 0.1$. We further measure the collision time τ, the mean free path λ, and the mean square displacement σ_v^2 of the vortices. We find the following laws: $\tau \sim t^{0.57}$, $\lambda \sim t^{0.45}$, and $\sigma_v^2 \sim t^{1.3}$. The statistics of passive particles (albeit virtual) in the system is also studied. They move hyperdiffusively, with an exponent similar to that obtained for the vortex motion. The dispersion of the particles is controlled by Lévy flights, produced by the jets formed by the dipoles. The distribution of flight times t_f is $t_f^{-2.6}$. Further analysis of the data indicates that the vortices undergo collisions whose geometrical aspects are analogous to those of an ordinary gas, and their motion is essentially Brownian diffusion in an expanding geometry. We finally underline the close relationship between the decay of turbulence and the dispersion phenomena. [S1063-651X(98)07410-8]

PACS number(s): 47.32.Cc, 47.27.Qb

I. INTRODUCTION

Two-dimensional (2D) turbulence has been considerably studied in recent years, because of its applications in astrophysics and geophysics, its relative accessibility to numerical computation, and as a fascinating field in its own right. The formation of coherent structures or vortices has been established both numerically and experimentally as a characteristic feature of 2D turbulent flows. In freely decaying turbulence, which is the issue we address here from an experimental point of view, the vortices tend to live long compared to their turnover time. From the time at which the coherent structures are formed, and until the final dipole state has been reached, the governing dynamical processes are the mutual advection of vortices, and the inelastic merging of like-sign vortices. In this time regime, assuming a self-similar evolution of the vortex system, and taking the energy per area E as the only invariant, one would find on dimensional grounds [1] that the density of vortices ρ decreases like $\rho \sim E^{-1} t^{-2}$. Numerical simulations, however, show a vortex number decay with a much slower rate [2–4]. To account for this observation, Carnevale *et al.* [3] proposed the extremum vorticity of the core of the vortices, ω_{ext}, as a second invariant. Assuming further that the vorticity is concentrated in vortices, they obtained the following scaling laws for the density of vortices ρ, the vortex radius a, the mean separation between vortices r, the velocity u of a vortex, the total enstrophy Z, and the kurtosis Ku of the vorticity distribution:

$$\rho \sim \mathcal{L}^{-2}\left(\frac{t}{\mathcal{T}}\right)^{-\xi}, \quad r \sim \mathcal{L}\left(\frac{t}{\mathcal{T}}\right)^{\xi/2}, \quad u \sim \sqrt{E},$$

$$Z \sim \mathcal{T}^{-2}\left(\frac{t}{\mathcal{T}}\right)^{-\xi/2}, \quad \mathrm{Ku} \sim \left(\frac{t}{\mathcal{T}}\right)^{\xi/2}, \tag{1}$$

in which the length scale $\mathcal{L}$ and time scale $\mathcal{T}$ are defined by

$$\mathcal{L} = \omega_{\mathrm{ext}}^{-1}\sqrt{E}, \quad \mathcal{T} = \omega_{\mathrm{ext}}^{-1}. \tag{2}$$

The exponent ξ is not determined by the theory. Numerical studies, both of the full Navier-Stokes equations and of point-vortex models, have consistently given values $\xi = 0.71$–0.75 [3,4]. On the experimental side, early investigations of the decay regime [5,6] confirmed that, as time increases, the vortex population becomes depleted and the mean vortex size increases. However, an accurate quantitative analysis of the phenomenon was not successfully achieved. Recently, two authors of the present paper made detailed measurements of the decay regime of quasi-two-dimensional flows [7]. However, in the system they explored, three-dimensional perturbations were suggested to play an important role. All this means that, at the moment, our knowledge of the phenomenon essentially relies on numerical studies.

Theoretically, several attempts have been made to determine ξ [8–11]. Based on the scaling laws (1), one of the authors of Ref. [4] proposed a derivation that yields $\xi = 1$, but argued for lowering corrections [8]. On the other hand, on the background of a theoretical approach using a probabilistic method to describe the motion of vortices in an external strain-rotation field, it has been suggested that the value of ξ depends on initial conditions [9]. In a related context, the 2D ballistic agglomeration of hard spheres with a size-mass relation mimicking the energy conservation rule for vortices, the value $\xi = 0.8$ is derived under mean-field assumptions [10]. Further, in another possibly related con-

*Permanent address: CATS, the Niels Bohr Institute, Blegdamsvej 17, 2100 København Ø, DK. Electronic address: aehansen@nbi.dk

text, that of Ginzburg-Landau vortex turbulence, the value $\xi=\frac{3}{4}$ has been proposed [11]. Despite these attempts, it is fair to say that a convincing theoretical argument determining the decay parameter ξ is still lacking.

Some of the theoretical attempts mentioned above bear on an analogy between the free decay of turbulence and the temporal evolution of populations of particles moving randomly and undergoing nonelastic collisions. At the moment, such an analogy has not been tested against experiment, to any extent. In particular, no measurements of the average time between two successive mergings and the corresponding vortex path lengths (which would represent the collision time and the mean free path, respectively) are available. The experimental approach to this question is indeed to study the displacement of the vortices, and since vorticity—to a certain extent—behaves as a passive scalar in 2D flows, this naturally leads one to address the general problem of dispersion of passive particles in freely decaying turbulence. This problem will thus be investigated in our paper. On the problem of dispersion in freely decaying turbulence, again no information is available at the present time. This situation contrasts with stationary two-dimensional forced systems, for which a few cases have been investigated in some detail. For randomly forced turbulence it has been found numerically [12] that the motion of passive particles is hyperdiffusive; the law of growth of the variance of the trajectories $\sigma^2 \sim t^\nu$ seems, however, to be characterized by a nonuniform behavior. Provided the existence of power laws is assumed (which may be questionable in some cases), it is found that the exponent ν jumps from 1.3 to 1.6 depending on whether the tracer visits hyperbolic or elliptic regions. Other stationary systems, dominated by coherent structures, have been studied experimentally, and several exponents—all hyperdiffusive—have been reported. For unclear reasons, most of them lie in the range $1.5<\nu<1.6$. This holds for flows in a rotating annular tank [13], flow in a vertically vibrated container for distances smaller than the wavelength of the surface waves [14], and drifters in the upper ocean [15].

The present paper reports an experimental investigation of vortex turbulence along with passive particle dispersion in a freely decaying 2D system. The paper is organized as follows. Turbulence is studied in Sec. III B, and compared to theoretical expectations. In Sec. IV the collision time for vortices, the mean free path, and the mean square displacement of the vortices are studied. In Sec. V the statistics of passive particles, obtained by a numerical integration of the experimentally determined velocity fields, is presented. We shall in particular analyze the particle trajectories for Lévy flights [16], using a general approach which has been found relevant in other systems [13,14,17]. We finally discuss the link between the dispersion and the decay problems, and suggest a physical picture for the decay of two-dimensional turbulence.

II. EXPERIMENTAL SETUP

A. Experiment

The experimental arrangement, shown in Fig. 1, is similar to the one used in previous studies by two of the present authors (see Ref. [7]). The flow is generated in a PVC cell, 20×27 cm^2. The bottom of the cell is a glass plate 1 mm thick. Permanent magnets of samarium cobalt, $5\times8\times3$ mm^3 in size, are located just below the glass plate; they are oriented so as to have a vertical magnetization axis. Each magnet produces a magnetic field of approximately 0.3 T.

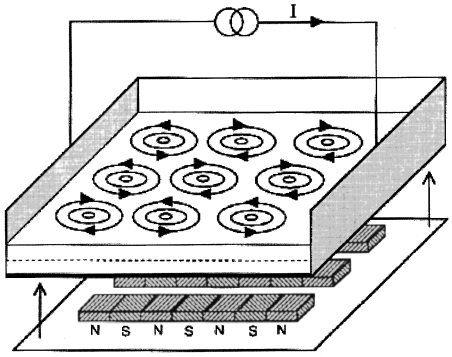

FIG. 1. The experimental setup (sketch).

The cell is filled with two layers of a solution of NaCl, of thickness 3 mm each. The layers have densities $\rho_1=1.14$ and $\rho_2=1.29$ g/cm^3, where the heavier fluid is on the bottom. The density difference of the interface acts to prevent vertical velocities, and thus bidimensionalizes the flow. It is only the use of stratification that distinguishes the experimental procedure from the one used in Ref. [7], but, as will be shown in Sec. III B, this additional precaution has a profound importance for the evolution laws of the vortices. The two-layer structure also provides a mechanism for a rapid transfer of vorticity from the bottom (where the magnets act most strongly) to the free surface. The vertical reorganization of the flow has a maximum duration of 2 s; thereafter the system can be regarded as two dimensional. However, as will be described in Sec. II B, the bottom friction still acts to give an overall exponential decay of the flow field. See Ref. [18] for a thorough experimental investigation of these matters which strongly justifies the bidimensionality of the setup, and Ref. [19] for numerical simulations which provide additional supporting evidence.

The flow boundaries in the horizontal plane are formed by solid rods of length 15 cm. The height of the rods equals the depth of the fluid, so as to prevent the formation of a meniscus. An electric current is driven through the cell from one side to the other, creating a force proportional to the current density which acts both horizontally and vertically on the fluid. The horizontal component of the forcing is dynamically active, while the vertical one is equilibrated by a pressure gradient. The structure of the initial flow is imposed by the arrangement of the magnets. The magnets are placed to create a 8×8 array of vortices, with nearest neighbors counter-rotating. Typical values of the current range from 200 mA to 1 A, the supply being controlled by a computer. The experimental procedure consists in imposing a constant electrical current I at time $t=-\tau$, switching it off at $t=0$, and letting the system relax. The initial value of the Reynolds number, calculated on the scale of the system, is typically $\mathrm{Re}=1800$.

B. Effect of bottom friction

In a transient time period of maximum duration 2 s after the forcing, the flow field reorganizes into a stationary verti-

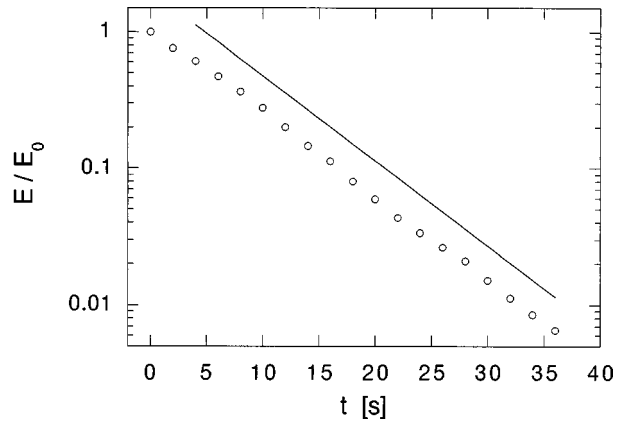

FIG. 2. The evolution of the system energy per area. Straight line: $e^{-0.14t}$.

cal profile [18]. Thereafter, the only effect of tridimensionality is the friction on the bottom of the cell, causing the energy to decay exponentially, $E=E_o\exp(-2\alpha t)$. In Fig. 2 we plot the evolution of the energy for a typical experiment. The time constant 2α agrees with the characteristic time for the relaxation of a Poiseuille profile $1/2\alpha=2b^2/\pi^2\nu$, where b is the total thickness of the fluid layer and ν is the kinematic viscosity.

The friction against the bottom can in the case of a stationary velocity profile be represented by a linear term in the 2D Navier-Stokes equations, or in terms of the vorticity $\omega(x,y)$,

$$\partial_t\omega+J(\omega,\psi)=\nu\nabla^2\omega-\alpha\omega, \tag{3}$$

where $\omega=-\nabla^2\psi$, and $J(\cdot,\cdot)$ is the Jacobian. In order to counterbalance this term we apply the transformation

$$\omega(w,y,t)\rightarrow\tilde{\omega}(x,y,t)e^{-\alpha t}, \tag{4}$$

and rescale the time as $\alpha t^*=1-e^{-\alpha t}$. One then arrives at

$$\partial_{t^*}\tilde{\omega}+J(\tilde{\omega},\tilde{\psi})=\nu^*\nabla^2\tilde{\omega}, \tag{5}$$

where $\nu^*=e^{\alpha t}\nu$. The flow is therefore equivalent to a two-dimensional flow with a time dependent viscosity. In the limit of high Reynolds numbers, it is legitimate to discard the temporal variation of the viscosity and confront the experimental results to pure two-dimensional systems using a constant viscosity.

All measurements of temporal properties will hereafter be expressed in terms of the transformed time t^*. Note that under the transformation the maximal observational time is $t^*_\alpha=1/\alpha$.

C. Determination of the velocity field and related quantities

The method of determination of the velocity field has also been described in a previous paper [7]; here we summarize its essential aspects. The flow is visualized using clusters of neutrally buoyant particles, several tens of microns in size. Those particles are made visible by illuminating the fluid from above with an halogen lamp. The images of the flow are captured with a video camera and recorded on a video tape.

During the decay process, an audio signal is generated on the sound channel of the video tape recorder, so as to identify each frame of the video signal. In a second step, the video frames are digitized, ordered, and recorded on magneto-optical disk. The method we use consists of discretizing the flow surface on a grid. For each node, we compute the correlation of the intensity field between two frames separated by a time interval δt on a box of size $l_c\times l_c$. The position of the maximum of the correlation provides information about the mean displacements of the pattern of illuminated particles. For the flow we consider, we use a 35 pixel/cm spatial resolution, and 40×40 measurement points. To correct clearly erroneous velocity vectors, the local divergence (or any ''test'' function of the derivatives) of the velocity field is computed and, if it exceeds some threshold value, we replace the aberrant value by the local average of the velocity. This occurs on average at three or four points in any velocity field.

The calculations are performed on a microcomputer, assisted by a double digital signal processor Digital Signal Processing 32C. To compute the local derivative and the vorticity field, we determine a polynomial fit for each component of the velocity v_x and v_y; the derivatives are calculated from the fit. In practice, we use a polynomial of degree 2. Compared to spectral techniques, this method has the advantage of conserving all the moments, up to the degree of the fitting polynomial.

When the velocity and vorticity fields are determined, we calculate the following three spatially averaged moments: the energy per area E, the enstrophy Z, and the kurtosis of the vorticity distribution Ku, as

$$E=\frac{1}{L^2}\int d\mathbf{x}\frac{\mathbf{u}^2}{2},$$

$$Z=\frac{1}{L^2}\int d\mathbf{x}\,\omega^2, \tag{6}$$

$$\mathrm{Ku}=\frac{1}{Z^2}\frac{1}{L^2}\int d\mathbf{x}\,\omega^4.$$

Furthermore, we determine the evolution of the geometrical properties characterizing the flow, namely, the number of vortices N, their mean radius a, and their mean separation r. To define a vortex, we search for values $|\omega(x,y)|$ of the vorticity field around a unique, local extrema ω_{ext} such that $\omega_{\mathrm{ext}}>|\omega(x,y)|>\omega_s$, where ω_s is a threshold. We use values of the threshold such that the initial number of vortices is correctly determined. In practice this gives a ratio $\omega_s/\omega_{\mathrm{ext}}\sim0.4$ to 0.6. We have verified that this method is in accordance with the *Weiss criterion* (see e.g., Ref. [20]) that associates the coherent structures to the areas of the flow with a negative determinant Q of the velocity gradients. Our procedure is an alternative to the rather constraining selection method of Ref. [2].

An example of how this procedure works is shown in Fig. 3. The characteristic vortex size a is found from the mean area occupied by the vortices. The mean distance r between the vortices is found by averaging over the distances between nearest neighbors.

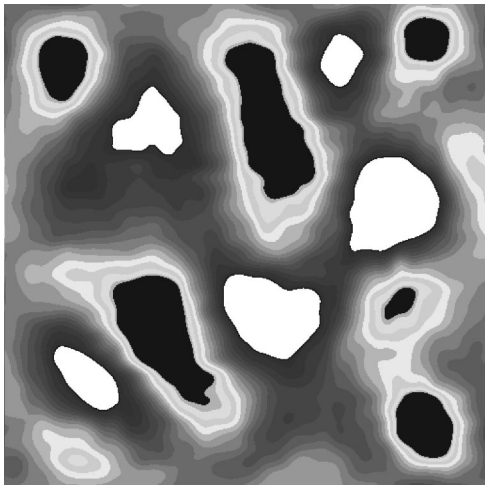

FIG. 3. An example of a vorticity field, illustrating the procedure used to identify the vortices. The areas identified as vortices, with the procedure described in the text, are colored uniformly. Areas colored white correspond to positive vorticity, and areas colored black to negative vorticity.

Finally, we study the dispersion of the vortices. The position of a vortex is defined by the position of the vorticity extremum. We measure the following quantities: the mean velocity u, the mean collision time τ, the mean free distance λ, and the mean squared displacement σ_v^2. The vortex velocity is calculated using a time step $dt=0.5$ s, which is 3–4 times larger than the intervals between the calculated vorticity fields, to avoid the influence of noise, due to the finite resolution. τ could also be called the mean ''lifetime'' of a vortex. It is the time between two subsequent mergings of the same vortex. If a close interaction between two like-sign vortices leads to the destruction of one of the vortices, then both vortices are judged to have undergone a merging. Then λ is the total displacement of the vortex center in this time interval. Additionally, we also measure λ_{tr}, defined as the length of the trajectory followed by the vortex center in the time interval in question. Likewise, we calculate the total mean square displacement σ_v^2 of the vortices (allowing for a vortex to merge on its way).

The typical time it takes for two like sign vortices to merge, is 5–10 times smaller than the time delay between successive mergings. We can thus treat the merging process as an instantaneous event.

For each time, the mean is obtained by averaging over the properties of all the vortices present in the system. In order to track the vortex centers continuously, the intervals between the calculated vorticity fields correspond to a small movement of the vortices, compared to the intervortex distance. We typically calculate 65–75 fields over the whole duration of the experiment.

D. Tracer statistics

To investigate the properties of passive particles moving with the fluid, we have performed numerical integrations of the trajectories of imaginary particles. For a chosen initial condition $\mathbf{x}(t=0)$, the trajectory $\mathbf{x}(t)$ is obtained by integrating the equation

$$\frac{d\mathbf{x}(t)}{dt}=\mathbf{v}(\mathbf{x},t). \tag{7}$$

The derivatives $\mathbf{v}(\mathbf{x})$ are given by the experimentally determined velocity fields. As above, the velocity fields are found with small, regular time intervals, to ensure that the velocities only change slightly. The 40×40 velocity fields are interpolated in space and time, and the trajectories are calculated using a standard fourth order Runge-Kutta method with adaptive stepsizing.

We find that this is an effective method for extracting statistical quantities from the flow fields. It allows us to average over a large number of trajectories, and thus to obtain statistics that would be difficult to achieve experimentally. The imaginary particles are indeed truly passive, so we do not have to consider the question of Stokes drag or similar experimental problems. On the other hand, since there is a limited resolution of the velocity field (0.375 cm between neighboring vectors), it is clear that the particles cannot correctly sample motions on a much smaller scale. To this point we remark that in any case the quantity we are interested in, namely, the mean square displacement σ^2 of the particles, is determined by the large scale properties of the flow (and already after 1 s the typical $\sqrt{\sigma^2}>0.7$ cm). In the calculations presented we use an ensemble of 3200 trajectories with initial conditions uniformly distributed over the experimental domain.

It turns out that the velocities of the particles vary a great deal according to which region of the flow a particle samples. In particular, as will be explained in Sec. V A, peaks in the particle velocities correspond to advection in regions between close, opposite-sign vortices. To make this observation quantitative, we have developed a procedure to analyze the trajectories for flight events; some examples of the procedure are shown on Fig. 4. The flights are determined by searching for extrema of the velocity above a threshold (taken as 0.80 cm/s, where the square root of the total, constant, system energy per unit area, is 0.71 cm/s). The beginning and end of a flight event are defined by the maximum and minimum in acceleration before and after a velocity extremum. The absolute value of the acceleration is required to be above another threshold (taken as 0.3 cm/s^2), ensuring that the flight corresponds to the time between when the particle enters and exits a flow region with high velocity. The conclusions stated in Sec. V remain valid for a variation of the above thresholds within $\pm15\%$. Events that do not start or stop within the finite duration of the trajectory are not counted; neither are events with their extremum velocity occurring in the first 2 s of the experiment.

We stress that there does not exist a universal algorithm to define flights of particles in hydrodynamical flows. We have checked for a large number of trajectories that our procedure correctly identifies the events, that strike an observer ''by eye'' as flights.

III. MEASUREMENTS OF TEMPORAL SCALING PROPERTIES

A. Qualitative aspects

The time evolution of the vorticity field in a typical experiment is displayed in Fig. 5. As explained in Sec. II A

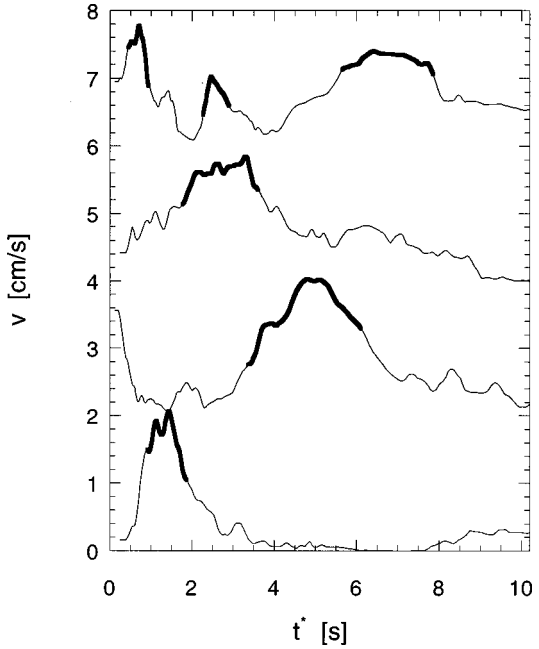

FIG. 4. Examples of flight identification. We show the velocities of single advected particles; regions defined as flights by the procedure described in Sec. II D are marked with a thick line. (There are added 2, 4 and 6 cm/s to the upper curves in order to separate the curves.)

above, we arrange the magnets such that the initial forcing produces an 8×8 array of vortices (upper image). Rapidly, like-sign vortices start to merge, almost exclusively with one of their initial nearest like-sign neighbors. Fewer and larger structures are thus formed, as one will see turning to the middle image, obtained after 5 s. Both well-formed vortices and pairs in the midst of a merging are visible. Dipole formation is in general observed throughout the decay, but these will usually not move very far—either because one of the vortices breaks off and merges with another vortex, or simply due to the constraining action of the field of the surrounding vortices. Finally, at $t=28$ s (lower image), the energy is so small that no further evolution of the vortices can be observed. With the initial large number of vortices, chosen to obtain good statistics in the decay regime, the limited experimental time (see Sec. II B) does not allow us to reach the final state. This is, however, possible starting with a smaller number of vortices, see Ref. [21].

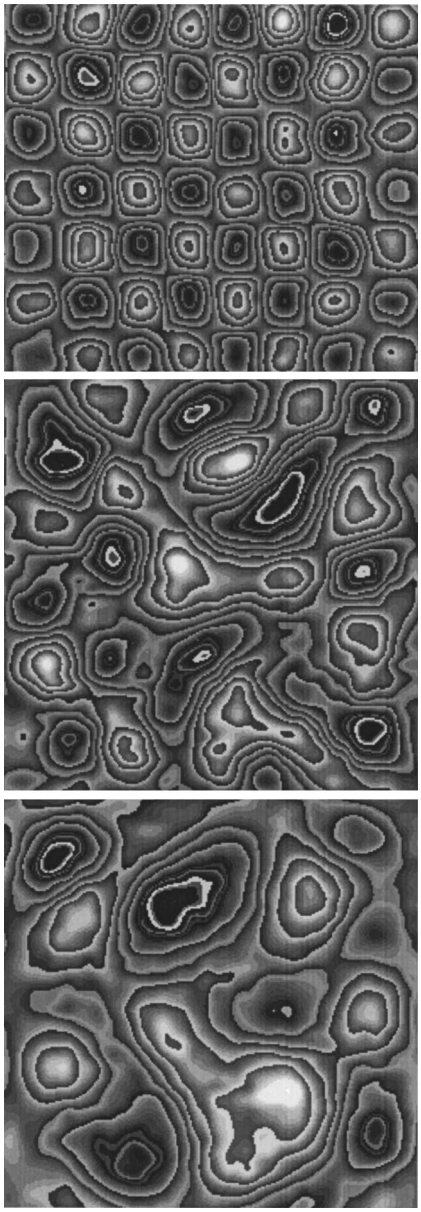

FIG. 5. Examples of calculated vorticity fields, showing the qualitative evolution of the flow from a large number of small vortices, to a smaller number of larger vortices. The overall exponential decline of the energy does not allow the final dipole state to be reached. Top: $t=0$ s (initial field). Middle: $t=5$ s. Bottom: $t=28$ s. Time is not rescaled here.

B. Scaling laws

We present measurements that are a mean over nine experimental realizations. In this system, remarkable, stationary features are apparent only for quantities averaged over some realizations. The fluctuations observed between individual realizations provide a basis to calculate an error bar. Figure 6 shows the evolution of the number of vortices obtained after ensemble averaging. A power law applies for the time period 1 s $<t^*<10$ s. Plotting the points on a semilog scale shows a clear incompatibility with an exponential law. Furthermore, when plotting the logarithmic slope of $N(t)$ (inset in Fig. 6) a plateau appears for the above time period, thus confirming the algebraic decay of the vortex number. Concerning the time period where the scaling is observed, one sees that for $t^*<1$ s the influence of the ordered initial conditions progressively gives way for a power law; for $t^*>10$ s the energy has diminished to a few percent of its initial value, and the vortices start to disappear compared to the experimental noise. In between, a power law takes place, and the corresponding exponent we find is

$$N=t^{-0.70\pm0.1}. \tag{8}$$

The error bar results from the variation in the included individual runs. We have checked that we obtain similar results, starting with 6×6 and 10×10 initial arrays of vortices.

Figure 7 represents geometrical characteristics of the system, i.e., the vortex radius, and their separation distance as a

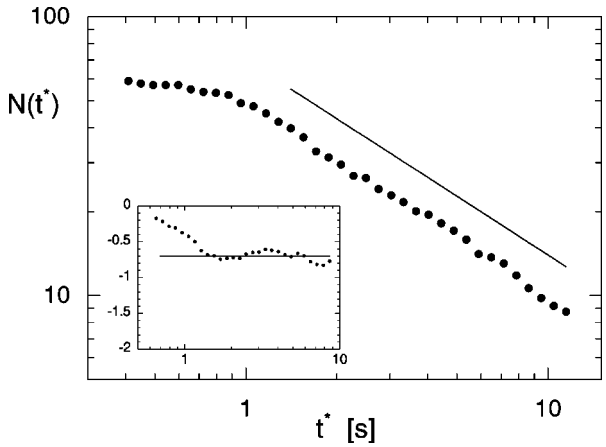

FIG. 6. Number of vortices vs time, average of nine realizations. Straight line: $t^{-0.7}$. Inset: logarithmic slope of the curve.

function of the rescaled time. Both quantities increase, showing that the geometry expands (albeit at slow rates) as time increases. For the period from $t=1.5$ to 10 s, we find the laws

$$\rho(t)\sim t^{-0.70\pm0.1},$$
$$a(t)\sim t^{0.21\pm0.06}, \tag{9}$$
$$r(t)\sim t^{0.38\pm0.08}.$$

Other quantities, the enstrophy and the kurtosis of the system, along with the extremum vorticity, are represented in Fig. 8 (the enstrophy and extremum vorticity are corrected for the overall exponential decline of the energy).

If power laws are assumed, for the period 2 s $<t<10$ s, they read

$$\frac{\omega_{\rm ext}}{\sqrt{E}}\sim t^{*-0.15\pm0.04},$$
$$\frac{Z}{E}\sim t^{*-0.47\pm0.06}, \tag{10}$$
$$\mathrm{Ku}\sim t^{*0.13\pm0.1}.$$

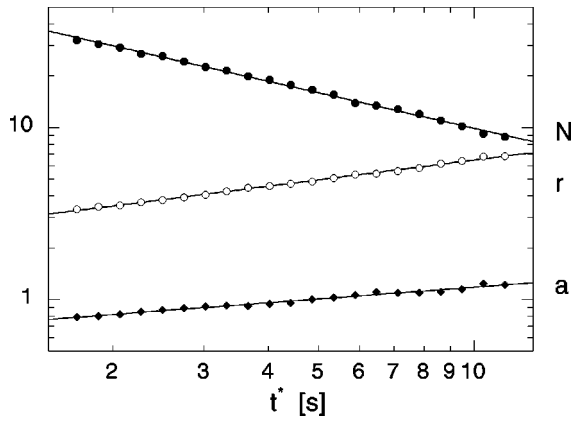

FIG. 7. Time evolution of geometrical quantities: density of vortices ρ, mean separation r, and mean radius a, as a mean of nine realizations. Straight lines: $t^{-0.7}$, $t^{0.38}$, and $t^{0.21}$.

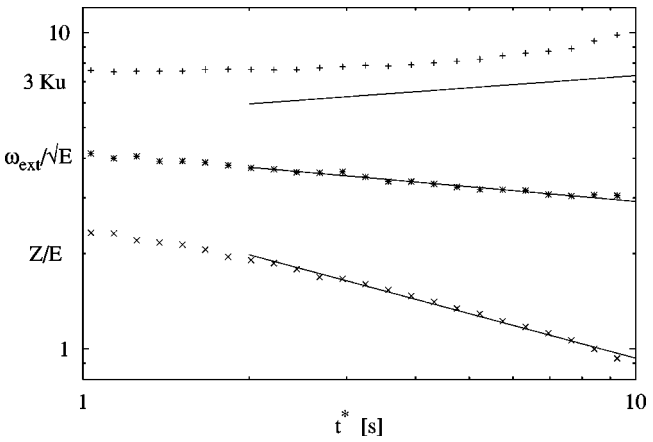

FIG. 8. Time evolution of dynamical quantities: extremum vorticity, enstrophy and kurtosis. Full lines: $t^{-0.15}$, $t^{-0.47}$, and $t^{0.13}$.

The conservation of the extremum vorticity is a basic assumption in the theory [3]. Here we find a slight decay, which is probably due to a finite Reynolds number effect (as seen as well in numerical studies [4]).

Let us now systematically compare our results to the theory [Eq. (1)]. If we take 0.70 ± 0.1 as the value defining the exponent ξ, we expect an exponent 0.18 ± 0.025 for the increase of the vortex size $a(t)$, and 0.35 ± 0.05 for the distance between vortex centers $r(t)$. These agree well with the experiment.

Another way to test the theory is to whether the internal relations proposed by the theory agree with the experiment. According to the theory, one should have

$$E=\rho\omega_{\rm ext}^2a^4, \quad Z=\rho\omega_{\rm ext}^2a^2.$$

In Fig. 9 we plot the ratios $E/\rho\omega_{\rm ext}^2a^4$ and $Z/\rho\omega_{\rm ext}^2a^2$. Within 10 %, plateaus are found, showing that the above relations hold in the experiment.

The laws for the kurtosis and the enstrophy, while having the right signs, are slower (faster) than the predictions [Eq. (1) gives $t^{0.35}$ for the kurtosis, and $t^{-0.35}$ for the enstrophy], and the power laws are not so well defined. The deviations can be interpreted in the framework of a finite-Re diffusive

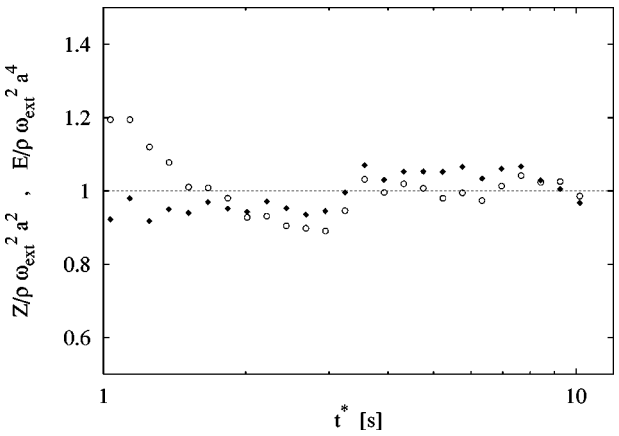

FIG. 9. Test of the expressions $E=\rho\omega_{\rm ext}^2a^4$ for the system energy (circles) and $Z=\rho\omega_{\rm ext}^2a^2$ for the enstrophy (diamonds). On plotting the ratios plateaus are formed.

effect [4], as for the extremum vorticity. Assuming a decay of extremum vorticity as $\omega_{\rm ext} \sim t^{-\nu}$, would alter the scaling equations (1) to

$$a \sim t^{\xi/4+\nu/2}, \quad \mathrm{Ku} \sim t^{\xi/2-\nu}, \quad Z \sim t^{-\xi/2-\nu},$$

under the condition that the average circulation of the flow remains constant under diffusion, which is approximately fulfilled in the experiments. This gives, in rescaled quantities and with $\nu = 0.15$, $a \sim t^{0.25}$, $\mathrm{Ku} \sim t^{0.20}$, and $Z/E \sim t^{-0.50}$. These exponents are indeed (for the enstrophy and the kurtosis) closer to the values seen in Eq. (10), and still acceptable for the radius a. However, we note that the algebraic laws are not so well defined for the enstrophy and especially not for the kurtosis: a probable reason for this is that at early times of the decay regime, the vortices are small and the accuracy of the measurement of these two quantities is low. To sum up, we find good agreement between the experimental results and the self-similar decay theory [4], the value of ξ being determined to $\xi = 0.70 \pm 0.1$ consistent with numerical estimates.

For completeness, we list here the prefactors involved in relation (9). Writing such relations in the forms

$$\rho \sim K_\rho \mathcal{L}^{-2} \left(\frac{t}{\mathcal{T}} \right)^{-0.70},$$

$$a \sim K_a \mathcal{L} \left(\frac{t}{\mathcal{T}} \right)^{0.21},$$

$$r \sim K_r \mathcal{L} \left(\frac{t}{\mathcal{T}} \right)^{0.38},$$

where $\mathcal{L}$ and $\mathcal{T}$ are given by Eq. (2), one obtains the estimates

$$K_\rho = 0.043,$$

$$K_a = 1.99,$$

$$K_r = 5.85.$$

These prefactors may have interest for a comparison with other experiments, and numerical simulations.

IV. MEAN FREE DISTANCE, COLLISION TIME, DIFFUSION COEFFICIENT

A. Measurements

Turning now to the dynamical features of the vortices, in Fig. 10 we show some typical vortex trajectories. These confirm the general impression (Sec. III A) that the vortices do not move far in the system.

In Fig. 11 we plot the quantities λ, λ_{tr}, and τ (as defined in Sec. II C) versus time on log-log scale. The data are from the same experiments as in Sec. III.

All three quantities grow as a power law for times 1.5 s $< t <$ 7 s, and with exponents that are close. We find the following laws:

$$\tau \sim t^{0.57 \pm 0.12}, \tag{11}$$

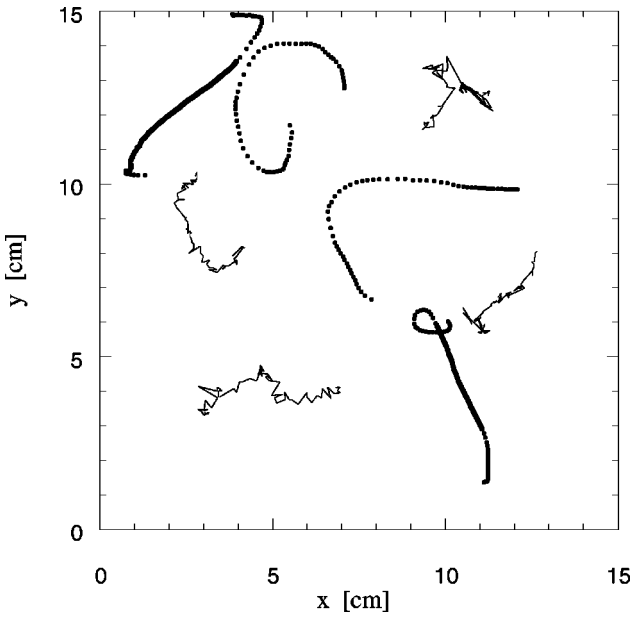

FIG. 10. Some trajectories of vortices (lines), and passively advected particles (points, with approximately equal time spacings. The analysis uses five times the shown resolution). Parts of particle trajectories defined as a flight are shown with a gray line (trajectories to the upper left and lower right).

$$\lambda_{tr} \sim t^{0.49 \pm 0.09},$$

$$\lambda \sim t^{0.45 \pm 0.10}.$$

Note that the prefactor for λ_{tr} is a factor of 3 smaller than the prefactor for λ, signifying an intricate movement of the vortices.

Indeed, one expects λ and τ to have the same behavior, since the mean velocity of the vortex centers is constant according to Eq. (1). For an explicit comparison, in Fig. 12 we plot the ratio λ/τ and the velocity u of vortex centers measured directly. Both quantities decrease slightly, however, the velocity approximately, as $t^{-0.07}$ in the above time interval.

In Fig. 13 we show σ_v^2, calculated for the 34 vortices tracked throughout the whole experimental time (they are

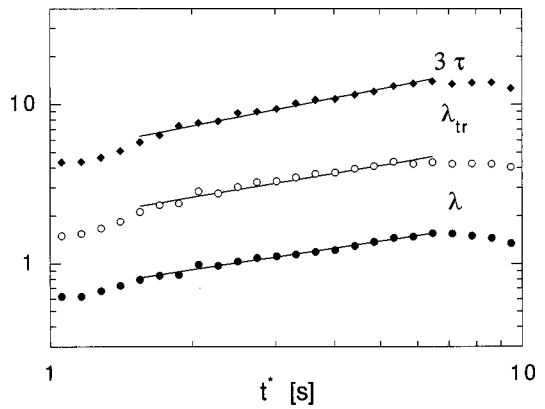

FIG. 11. Time evolution of the mean free distance λ, the mean free distance measured by the length of the trajectories between mergings λ_{tr}, and the collision time τ. Straight lines: $t^{0.49}$, $t^{0.45}$, and $t^{0.57}$.

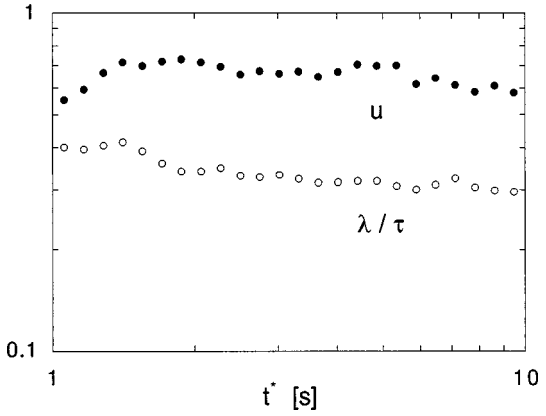

FIG. 12. Ratio λ/τ, and the vortex velocity u.

allowed to undergo mergings). A well-defined power law is observed. For the time interval 1.2 s$< t <$ 7 s, we find

$$\sigma_v^2 \sim t^{1.3\pm 0.1}. \tag{12}$$

So the vortices move hyperdiffusively.

B. Discussion

The exponents observed can be understood in terms of a simple geometrical argument. Estimate λ as the distance traveled by a vortex in unit time ($\sim u$, the invariant advection velocity), divided by the probability of suffering a collision in this time interval ($\sim u$ times the collisional cross section times the density of vortices). Then

$$\lambda \sim \frac{u}{u\sigma\rho} \sim \frac{1}{\rho a}, \tag{13}$$

since the collisional cross section is proportional to the radius for a system of circular disks. The collision time τ is simply

$$\tau \sim \frac{\lambda}{u} \sim \frac{1}{\rho a u}. \tag{14}$$

Inserting the algebraic laws for the time evolution of a and ρ, one arrives at

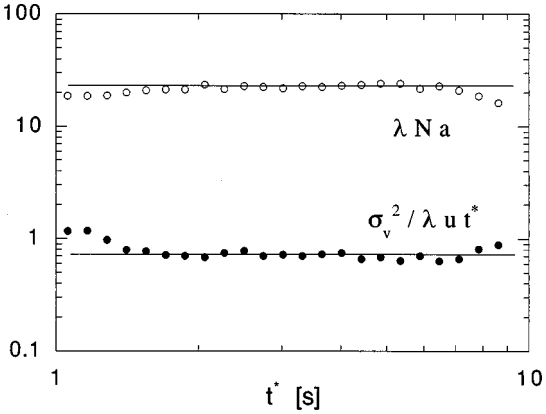

FIG. 13. The mean square displacement of the vortices σ_v^2, calculated for 34 vortex trajectories. Straight line: $t^{1.3}$.

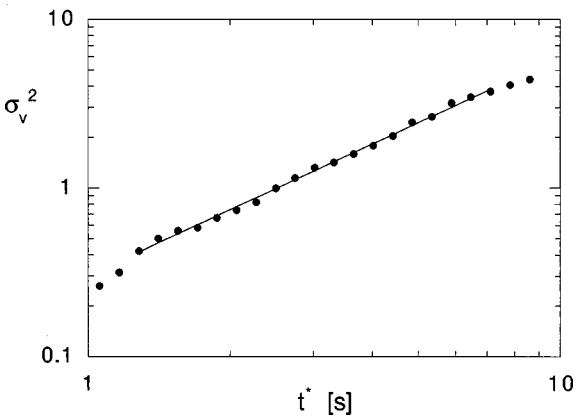

FIG. 14. Invariants λNa and $\sigma_v^2/\lambda u t^*$. Straight lines are shown for comparison.

$$\lambda \sim \tau \sim t^{\xi} t^{-(1/4)\xi} \sim t^{(3/4)\xi}. \tag{15}$$

With the obtained value $\xi = 0.7$, we should have $\tau \sim \lambda \sim t^{0.5}$, which is in agreement with the observed power laws (11).

To further test Eq. (13), in Fig. 14 we plot the product λNa, as given by the data. A clear plateau is observed for times 1.5 s $< t <$ 7 s, corresponding to the scaling regime of λ.

On the whole, we conclude that expressions (13) and (14) for λ and τ are confirmed by experiment. The power law for σ_v^2 can be understood as follows: introduce a vortex diffusion coefficient D by

$$\sigma_v^2 \equiv Dt. \tag{16}$$

Estimating D as the mean free path squared divided by the collision time gives

$$D = \lambda u. \tag{17}$$

Thus the growth in length scale causes D to grow as well. Further, the mean square displacement of the vortices σ_v^2 is now given by

$$\sigma^2 \sim Dt \sim \lambda u t. \tag{18}$$

If D had been constant, one would have that $\sigma_v^2 \sim t$, that is, Brownian motion of the vortices. But now D increases with time, and in turn the variance grows faster than t. Equation (18) can be further tested directly, by plotting $\sigma_v^2/(\lambda u t)$ versus time (see Fig. 14). A plateau appears for times larger than 1.5 s, so Eq. (18) is well verified by experiment.

It is tempting to infer, from the above relations, a formula between ξ and an exponent characterizing the temporal evolution of the mean square displacement of the vortex centers. From Eqs. (13) and (18), one may deduce that if σ_v^2 grows as t^{ν}, one must have the following relations between ξ and ν:

$$\nu = 1 + \tfrac{3}{4}\xi. \tag{19}$$

By taking $\xi = 0.7$, one should find the mean square displacement of the vortices is characterized by an exponent equal to 1.5. This is a bit larger than the observed exponent, which is 1.3; the reason is that systematic errors add so as to violate

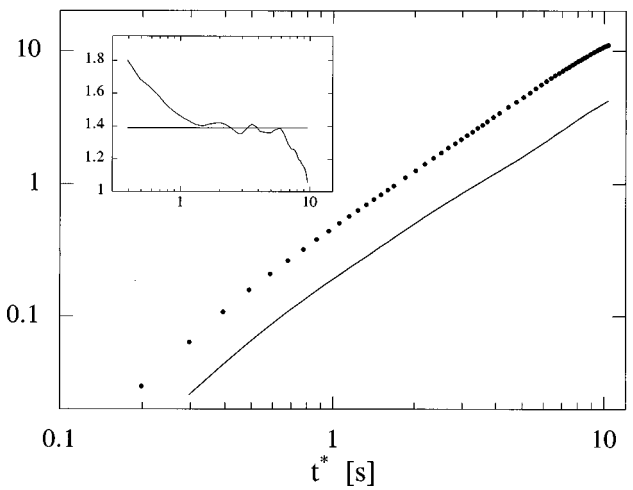

FIG. 15. The mean square displacement of 3200 passive, imaginary particles (circles) and a subset of 2208 particles not entering high-vorticity regions (line). The latter curve has been divided by 2. The two curves are almost indistinguishable. Inset: the logarithmic slope of the overall mean.

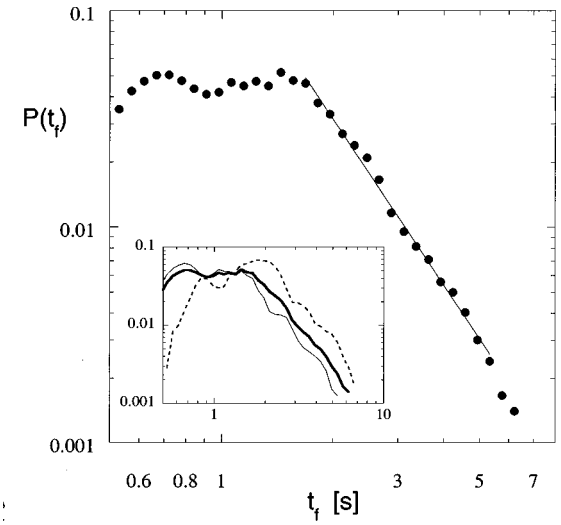

FIG. 16. Probability distribution of flight times. Straight line: $t_f^{-2.56}$. Inset: the same distribution (thick line), along with the distribution of flights with extremum velocity occurring between $t^*=2-5$ seconds (thin line), and $t^*=5-10$ s (dotted line).

Eq. (19). The main factor is that u is not exactly constant, but slightly decreases with time. In practice, one can say that relations (13) and (18) are consistent with the experiment, and the corresponding straightforward relation (19) must be taken as an approximate formula expressing the existence of a link between the exponent characterizing the decay, and that characterizing the dispersion of the vortices in the experiment.

V. DISPERSION OF PASSIVE PARTICLES

In this section, we present studies of the dispersion of passive, imaginary particles, where the trajectories are obtained as described earlier in Sec. II D. To demonstrate the qualitative behavior of the particle motion, in Fig. 10 we show some examples of particle trajectories. We note that trapping effects are not visible. Particles can enter vortices during mergers, and, surely for some of the random initial conditions, begin in the core of the vortices, but the particles tend to be rapidly ejected, both during mergers and as an effect of the straining of vortices due to the surrounding field. The observation that the vortex cores are characterized by a low tracer density is in qualitative accordance with Ref. [12]. Here we want to make it clear that trapping in vortices and sticking on their periphery are not effects that seems important for the particle dispersion; indeed, well-defined trappings are too rare to justify a detailed analysis. Flights, or parts of the trajectories with a velocity persistently higher than the mean velocity, are, on the other hand, often observed.

In Fig. 15 we show the mean of the absolute squared displacement σ^2 of the particles. A clear power law emerges for times between 1 and 7 s. The detailed nature of the dispersion can be appreciated in the inset, which shows the logarithmic derivative of the preceding points. For small times, the exponent decreases from 1.8, while, from $t=6$ s, the exponent drops to 1. The small and large time behavior is thus in accordance with the classical prediction [22]. However, the change in exponent is not smooth, but shows a clear plateau, thus defining a dispersion coefficient for intermediate times, with the value $\sigma^2 \sim t^{1.39}$. As a mean over three experiments, we find

$$\sigma^2 \sim t^{1.4\pm0.1}. \tag{20}$$

It is remarkable that this exponent is indistinguishable from that corresponding to the mean square displacement of the vortex centers.

Characterization in terms of flights

To trace the origin of the hyperdiffusion observed for passive, imaginary particles, we have analyzed the computed tracks for flight events, as described in Sec. II D. The flight time distribution in Fig. 16 is a result of this procedure. 5700 particle tracks have been analyzed, giving a total of 4400 flight events. For flights longer than 1.5 and less than 6 s, the distribution follows a power law. For long flights, the statistics will be influenced by the finite duration of the trajectories (recall that the total duration of the experiment is 10.4 s); this explains the rapid decrease in $P(t_f)$ for $t_f > 6$ s. We conclude that the distribution of flight times has an algebraic tail, with a law given by

$$P(t_f) \sim t_f^{-2.6\pm0.2}. \tag{21}$$

We have investigated the temporal evolution of the characteristics of this distribution; this is shown in the inset of Fig. 16. The plot also shows the same analysis, but performed over a smaller range of time, so as to see how the characteristics of the distribution evolves with time. Although the statistics is on the border of being sufficient to draw reliable conclusions, it seems that the tails stay parallel to each other as time increases, which means that the slope of the distri-

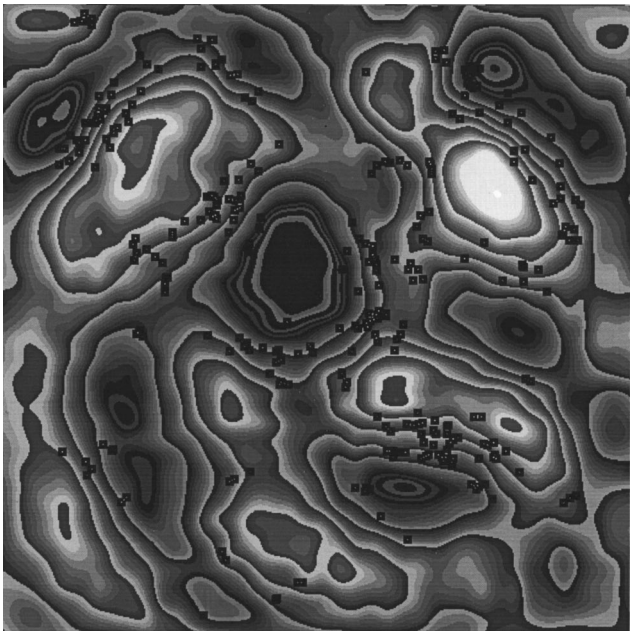

FIG. 17. Vorticity field to $t=8.5$ s. The positions of particles undergoing a flight are marked with black squares.

bution does not vary with time. It thus seems that the distribution are not sensitive to the fact that the system expands.

We have also investigated in which regions of the flow the particles move when they are subject to a flight. As demonstrated in Fig. 17, flights predominantly occur for particles located between opposite-sign vortices. This is not surprising, since the regions between two close opposite-sign vortices are characterized by large velocities, forming a jetlike structure. Thus there is a straightforward physical explanation for the occurrence of flights.

The exponents we find for the flight distribution are consistent with those for the variance. According to Ref. [16], we effectively have $\sigma^2 \sim t^{4-2.6} \sim t^{1.4}$, in good agreement with the previous result [Eq. (20)]. This shows that we can regard the hyperdiffusion for the passive particles as anomalous, that is caused by extreme (flight) events.

VI. DISCUSSION AND CONCLUSION

Let us first underline the good agreement between the experimental results obtained in Sec. III B and the theoretical predictions and previous numerical studies [3,4]. For the geometrical quantities, the agreement is excellent, and the value of $\xi = 0.7 \pm 0.1$ is close to the numerical estimates.

For the dynamical quantities, the enstrophy and the kurtosis, the behavior is close to the prediction of the scaling theory, when including a diffusive decay of the extremum vorticity [4]. Deviations are probably due to lack of resolution at early times in the experiment. In conclusion, our experimental results largely confirm the analysis of [3].

We have further investigated new quantities, such as the collision time scale of the vortices and the vortex diffusion coefficient, with good confirmation from measurements. Thus we have successfully characterized the dynamical behavior of the vortices, which is shown to be hyperdiffusive. The origin of this lies in the general scale dilation in the algebraically decaying vortex system. The picture we propose thus suggests that, as far as dispersion is concerned, vortices essentially behave like particles of an ordinary two-dimensional gas in an expanding geometry.

Incidently, the power laws governing the mean free path λ and the collision time τ deserve a few comments. It has been proposed that a collision time τ' can be defined from the equation $dN/dt = -N/2\tau'$. τ' measures the mean time by which the population of vortices has decreased by one half. Defined in this way, τ' is proportional to t, whatever the exponent at hand in the expression of $N(t)$. The collision time τ we measure increases with time at a slower rate. But τ' correspond to another kind of average, and it is not clear whether it defines a quantity of dynamical relevance for the problem at hand.

The exponent we find for the collision time can be further applied to a few theoretical attempts; in Ref. [8], it was proposed that $\tau_{\mathrm{coll}} \sim t^{\xi}$, not in agreement with our measurements [Eq. (11)]. In the context of 2D ballistic agglomeration of hard spheres with a size-mass relation mimicking the energy conservation rule for vortices [10], a relation answering Eq. (13) holds in numerical simulations [23]. But, as a consequence of a decreasing velocity of the aggregates, the collision time scale grows proportionally to t^1, making the analogy difficult. One may also mention that a relation between the decay parameter ξ and the vortex dispersion exponent ν was been proposed recently [24]. The expression is $\nu = 2 - \xi/2$. It turns out, however, that for the observed values $\xi = 0.7$ and $\nu = 1.3$, this relation does not agree with the experiment.

Having proposed that the vortices essentially diffuse in an expanding geometry, we have, with a seminumerical method, examined the motion of passive particles in the system. These move hyperdiffusively, and we have shown the presence of Levy flights, controlled by the jets formed by the dipoles. We thus have a nonuniformity of the physical processes at work: the particles linked to the highest vorticity levels undergo Brownian motion in a dilating geometry, while those visiting the background undergo stationary Levy flights. The fact that two different diffusion processes hold in the same system is conceivable on physical grounds. The highest vorticity levels are linked to structures of appreciable spatial extent, affected by the collective action of several neighboring vortices, whereas individual particles are sensitive to the local flow produced by individual structures or pairs of structures. The remarkable fact is that, despite the different physical mechanisms at work, both processes are characterized by the same exponent 1.3 ± 0.1. In freely decaying turbulence, the whole dispersion process seems to be characterized by a single exponent. We may finally underline the close relationship between the decay and the dispersion problems, expressed by relation (19); in a situation where Levy flights control the dispersion process, ν is expected to range between 1 and 2, so that the domain of variation of ξ extends between 0 and $\frac{4}{3}$. This illustrates that the dispersion processes may restrict the range of possible values for ξ. Stated differently, the fact that the vortices cannot move in an arbitrary way induces constraints on the decay regime of turbulence. One may ask whether such constraints are strong enough to select a particular value of ξ.

ACKNOWLEDGMENTS

This work was supported by Ecole Normale Supérieure, Universités Paris 6 et Paris 7, Center National de la Recherche Scientifique. The authors wish to thank A. Fairhall, B. Legras, O. Cardoso, J. Paret, E. Trizac, A. George, X. He, M. F. Schlesinger, J. Klafter, I. M. Sokolov, Y. Pomeau, A. Babiano, and G. Zaslavsky for interesting discussions concerning this work.

[1] G. K. Batchelor, Phys. Fluids Suppl. II **12**, 233 (1969).
[2] J. C. McWilliams, J. Fluid Mech. **219**, 361 (1990).
[3] G. F. Carnevale, J. C. McWilliams, Y. Pomeau, J. B. Weiss, and W. R. Young, Phys. Rev. Lett. **66**, 2735 (1991).
[4] J. B. Weiss and J. C. McWilliams, Phys. Fluids A **5**, 608 (1992).
[5] Y. Couder, C. R. Acad. Sci. URSS **297**, 641 (1983).
[6] E. Hopfinger, R. W. Griffiths, and M. Mory, J. Mec. Theor. Appl. **2**, 21 (1983).
[7] O. Cardoso, D. Marteau, and P. Tabeling, Phys. Rev. E **49**, 454 (1994).
[8] Y. Pomeau, J. Plasma Phys. **56**, 3 (1996); **56**, 407 (1996).
[9] X. He, in *Advances in Turbulence VI*, edited by S. Gavrilakis *et al.* (Kluwer, Dordrecht, 1996), p. 277.
[10] E. Trizac and J.-P. Hansen, Phys. Rev. Lett. **74**, 4114 (1995): J. Stat. Phys. **82**, 5/6 (1996).
[11] G. Huber, P. Alstrøm, Physica A **195**, 448 (1993).
[12] D. Elhmaïdi, A. Provenzale, and A. Babiano, J. Fluid Mech. **257**, 533 (1993).
[13] T. H. Solomon, E. R. Weeks, and H. L. Swinney, Physica D **76**, 80 (1994).
[14] A. E. Hansen, E. Schröder, P. Alstrøm, J. S. Andersen, and M. T. Levinsen, Phys. Rev. Lett. **79**, 1845 (1997).
[15] B. G. Sanderson and D. A. Booth, Tellus, Ser. A **43A**, 334 (1991); A. Provenzale, A. R. Osborne, A. D. Kirwan, and L. Bergamasco, in *Nonlinear Topics in Ocean Physics*, edited by A. R. Osborne (Elsevier, Amsterdam, 1991), p. 367.
[16] J. Klafter, A. Blumen, and M. F. Schlesinger, Phys. Rev. A **35**, 3081 (1987).
[17] O. Cardoso, B. Gluckmann, O. Parcollet, and P. Tabeling, Phys. Fluids **8**, 209 (1996).
[18] J. Paret, D. Marteau, O. Paireau, and P. Tabeling, Phys. Fluids **9**, 2752 (1997).
[19] B. Jüttner, D. Marteau, P. Tabeling, and A. Thess, Phys. Rev. E **55**, 5479 (1997).
[20] J. C. McWilliams, J. Fluid Mech. **146**, 21 (1984).
[21] D. Marteau, O. Cardoso, and P. Tabeling, Phys. Rev. E **51**, 5124 (1995).
[22] G. I. Taylor, Proc. London Math. Soc. **20**, 196 (1921).
[23] E. Trizac (private communication).
[24] X. He, Physica D **95**, 163 (1996).